

# Ultrafast Carbon Dioxide Sorption Kinetics Using Lithium Silicate Nanowires

Apolo Nambo,<sup>†,‡</sup> Juan He,<sup>‡</sup> Tu Quang Nguyen,<sup>‡</sup> Veerendra Atla,<sup>†</sup> Thad Druffel,<sup>†</sup> and Mahendra Sunkara<sup>\*,†,§</sup>

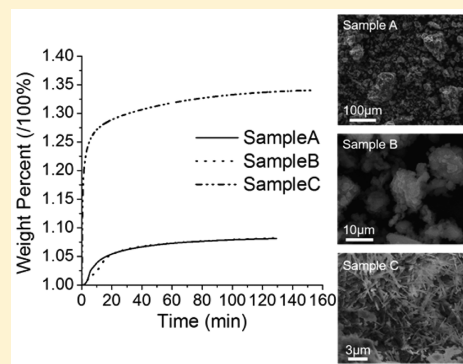
<sup>†</sup>Conn Center for Renewable Energy Research, University of Louisville, Louisville, Kentucky 40292, United States

<sup>‡</sup>Advanced Energy Materials, LLC, 311 E. Lee St., Louisville, Kentucky 40208, United States

## S Supporting Information

**ABSTRACT:** In this paper, the  $\text{Li}_4\text{SiO}_4$  nanowires (NWs) were shown to be promising for  $\text{CO}_2$  capture with ultrafast kinetics. Specifically, the nanowire powders exhibited an uptake of  $0.35 \text{ g g}^{-1}$  of  $\text{CO}_2$  at an ultrafast adsorption rate of  $0.22 \text{ g g}^{-1} \text{ min}^{-1}$  at  $650\text{--}700 \text{ }^\circ\text{C}$ . Lithium silicate ( $\text{Li}_4\text{SiO}_4$ ) nanowires and nanopowders were synthesized using a “solvo-plasma” technique involving plasma oxidation of silicon precursors mixed with lithium hydroxide. The kinetic parameter values ( $k$ ) extracted from sorption kinetics obtained using NW powders are 1 order of magnitude higher than those previously reported for the  $\text{Li}_4\text{SiO}_4\text{--CO}_2$  reaction system. The time scales for  $\text{CO}_2$  sorption using nanowires are approximately 3 min and two orders magnitude faster compared to those obtained using lithium silicate powders with spherical morphologies and aggregates. Furthermore,  $\text{Li}_4\text{SiO}_4$  nanowire powders showed reversibility through sorption–desorption cycles indicating their suitability for  $\text{CO}_2$  capture applications. All of the morphologies of  $\text{Li}_4\text{SiO}_4$  powders exhibited a double exponential behavior in the adsorption kinetics indicating two distinct time constants for kinetic and the mass transfer limited regimes.

**KEYWORDS:**  $\text{Li}_4\text{SiO}_4$ ,  $\text{CO}_2$ , adsorbent, nanowire, solvo-plasma



Around 85% of world's energy supply comes from fossil fuels.<sup>1</sup> The combustion of fossil fuels such as coal, oil, and natural gas mainly supports the energy demands of our society.<sup>2</sup>  $\text{CO}_2$  and other effluent greenhouse gases (GHGs) thus released pose enormous environmental challenges, such as global warming.<sup>1</sup> Therefore, the separation, recovery, and storage/utilization of  $\text{CO}_2$  has been drawing tremendous attention in recent years.<sup>3</sup>  $\text{CO}_2$  can be removed from flue gas and waste gas streams by various methods, such as membrane separation, absorption with solvent, and adsorption.<sup>4</sup> These technologies would help in the transition from the current use of fossil fuels to more clean energy sources in the future.<sup>5</sup>

The capture of  $\text{CO}_2$  onto solid sorbents is receiving increasing attention. Some materials of interest include zeolites, porous polymers, ion exchange resins, nanofibrillated cellulose, metal–organic frameworks, hydroxalites, amines, polymeric membranes, metal oxides, and different lithium ceramics.<sup>6,7</sup> In recent years, different lithium ceramics have been tested as possible  $\text{CO}_2$  adsorbents.<sup>8</sup> In fact, two of the most important properties of this kind of ceramics are the following: (1) The  $\text{CO}_2$  chemisorption can be performed in a wide range of temperatures up to  $650\text{--}710 \text{ }^\circ\text{C}$ ,<sup>3</sup> and (2) several of these ceramic materials are recyclable.<sup>9</sup>

Of all lithium ceramics, lithium silicates and zirconates have been extensively investigated as  $\text{CO}_2$  sorbents.<sup>10</sup> Of these two systems,  $\text{Li}_4\text{SiO}_4$  adsorbs more than 50% by weight  $\text{CO}_2$

relative to  $\text{Li}_2\text{ZrO}_3$  and does so at rates 30 times faster.<sup>11,12</sup> Several  $\text{CO}_2$  capacities have been reported for  $\text{Li}_4\text{SiO}_4$ , with a wide range of analysis conditions. For example, one study reported an uptake of 30.3 wt % after 95 min at  $620 \text{ }^\circ\text{C}$  with 100 mL/min flow of  $\text{CO}_2\text{:N}_2$  1:1,<sup>3</sup> while another found an uptake of 16.3 wt % after 160 min at  $560 \text{ }^\circ\text{C}$  in 150 mL/min flow of pure  $\text{CO}_2$ .<sup>9</sup>

$\text{Li}_4\text{SiO}_4$  preparation has been found to be critical in determining its structure, composition, performance, and use in potential applications. A solid state reaction is widely used for the production of  $\text{Li}_4\text{SiO}_4$ .<sup>13</sup> Here, solid mixtures of amorphous silica ( $\text{SiO}_2$ ) and a lithium compound (e.g.,  $\text{Li}_2\text{CO}_3$ ,  $\text{LiOH}$ ) are heated in air for long periods between 370 and  $1000 \text{ }^\circ\text{C}$  to produce lithium silicate powders. Other techniques include sol–gel and hydrothermal techniques, which also take about several hours of reaction time.<sup>14</sup> Many of these techniques yield lithium silicates with surface areas ranging from  $1 \text{ cm}^2/\text{g}$  to  $2.5 \text{ m}^2/\text{g}$ , consisting of aggregates of micron/macro scale particles.<sup>15,16</sup> The wide variations in the characteristics of the obtained products prevent the fundamental

**Received:** September 25, 2016

**Revised:** April 22, 2017

**Published:** May 23, 2017

determination of the factors affecting CO<sub>2</sub> sorption capacity and kinetics.

In this study, a new approach termed “solvo-plasma” (Figure 1) is investigated to prepare lithium silicate materials with

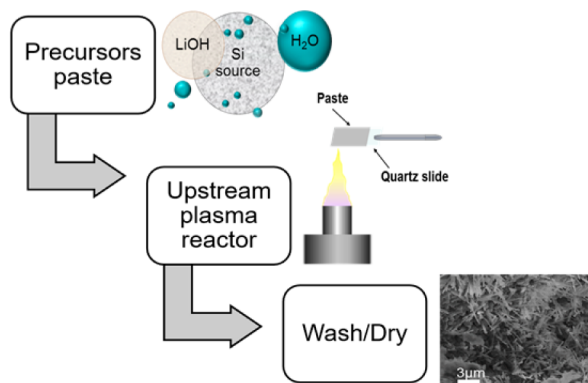
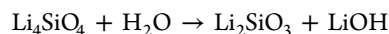


**Figure 1.** A schematic illustration of various steps used in our solvo-plasma synthesis method.

different nanostructured morphologies, including nanoparticles, sheet-like structures, and nanowires. The technique is based on our prior work on plasma oxidation with alkali salts for synthesizing one-dimensional materials with fast time scales.<sup>17</sup>

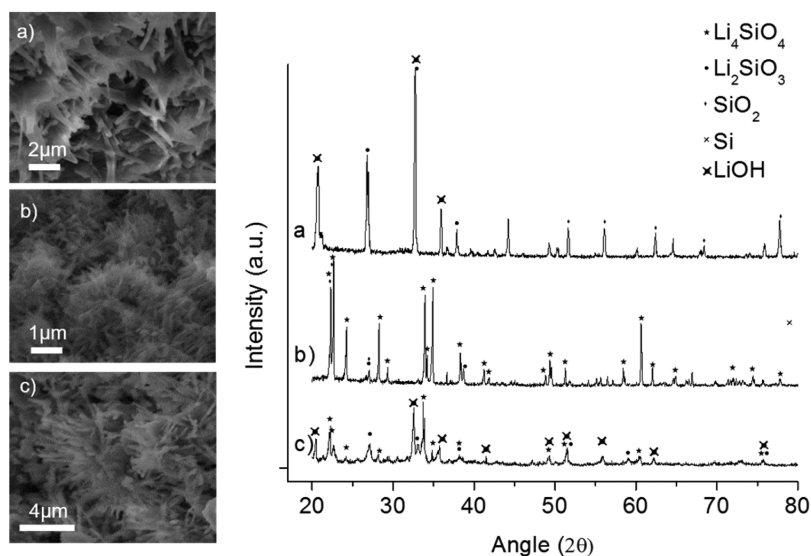
In general, several synthesis experiments were performed using thermal oxidation, microwave heating, and plasma oxidation of mixtures containing various ratios of silicon precursors and lithium hydroxide. Thermal oxidation experiments were performed using a furnace at 650 °C with 2 h duration. Microwave heating experiments were performed with 5 min duration using a commercial 1 kW microwave oven. Plasma oxidation experiments were performed using an upward atmospheric microwave plasma flame as shown in Figure 1 with powers ranging from 750 to 1200 W and for durations of around 1 min. All of the experiments utilized mixtures containing Li to Si about 4:1 or higher. The experiments are all summarized in Table S1 in Supporting Information (SI). All

three of the above techniques produced nanowire morphologies, but the main differences are with durations, resulting phases, and the amount of excess LiOH required. See the SEM images in Figure 2. The main difference is that the plasma oxidation approach is the only one that exhibited the predominant formation of Li<sub>4</sub>SiO<sub>4</sub> phase nanowires using Li to Si at molar ratios >4. The thermal oxidation method required Li:Si molar ratios greater than 12:1 to obtain Li<sub>4</sub>SiO<sub>4</sub> phase nanowires with 2 h duration. The microwave heating method resulted in the formation of Li<sub>2</sub>SiO<sub>3</sub> phase nanowires. See XRD data in Figure 2. This is because of the presence of water during heating triggered the following reaction:



In all of the methods, the mixtures of lithium hydroxide and silicon precursor powders melt upon heating using thermal or microwave heating or plasma exposure to form a molten Li<sub>x</sub>Si<sub>y</sub>O<sub>z</sub> phase. Subsequent oxidation of the molten phase results in the nucleation and growth of nanowires similar to our previous work in the case of tin oxide and titania nanowires.<sup>17,18</sup> Radicals and ions produced in the plasma flame play a key role in the fast nucleation and growth kinetics of Li<sub>4</sub>SiO<sub>4</sub> phase.

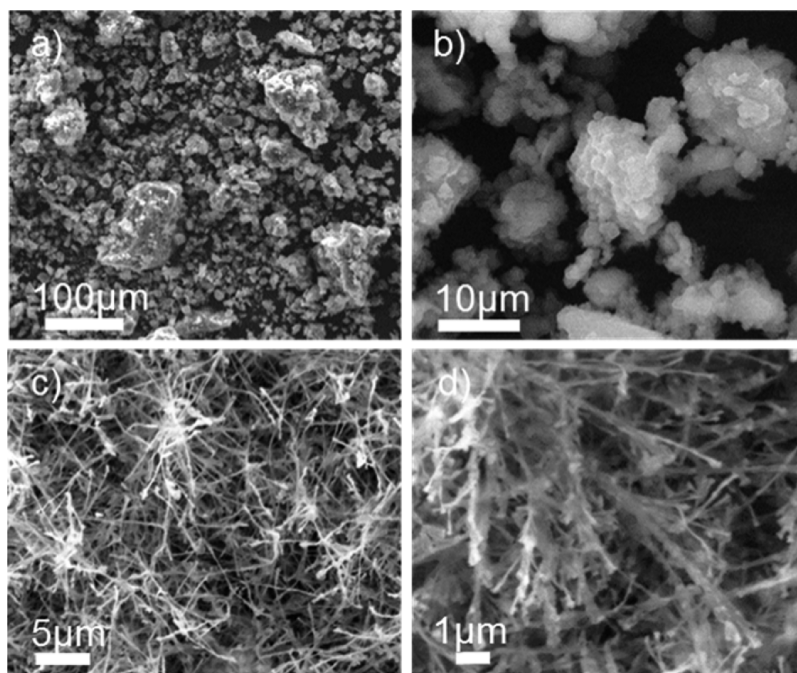
The Li<sub>4</sub>SiO<sub>4</sub> nanoparticles and nanowires produced using the plasma oxidation method were characterized and tested for CO<sub>2</sub> adsorption to understand the basic relation between the nanoscale morphology and the sorption kinetics. The XRD patterns of obtained samples are shown in Figure S2 in the SI. The pattern displayed typical reflection peaks expected for monoclinic Li<sub>4</sub>SiO<sub>4</sub> phase with lattice parameters of  $a = 5.3 \text{ \AA}$ ,  $b = 6.1 \text{ \AA}$ , and  $c = 5.14 \text{ \AA}$  and the space group of  $P21/m$ . In addition to the presence of Li<sub>4</sub>SiO<sub>4</sub> phase, the XRD pattern indicates the presence of unreacted precursors and the Li<sub>2</sub>SiO<sub>3</sub> phase. For all of the samples prepared, the principal reflections (011), (110), and (021), with  $2\theta$  angles of 22.2, 22.6, and 33.8, respectively, were monitored for several samples synthesized using different conditions (air plasma power, time of exposure, and precursors concentration) as an indicator of yield. Within this work, three different samples are presented: sample A consists of a material made using milled SiO<sub>2</sub> powder, a molar



**Figure 2.** SEM images of lithium silicate powders obtained: (a) Microwave heating using LiOH–Si at a molar ratio of 12:1, a microwave power of 1 kW and 5 min duration; (b) thermal oxidation using LiOH–Si at a molar ratio of 12:1, temperature of 650 °C, and 2 h duration, and (c) plasma oxidation using LiOH–Si at a molar ratio of 8:1, a microwave power of 750 W, and 1 min duration. (d) XRD patterns for the three samples.

Table 1. Morphological Properties and Performance of  $\text{Li}_4\text{SiO}_4$  Based Adsorbents from Dynamic Thermographs

lithium silicate	morphology	BET surface area ( $\text{m}^2/\text{g}$ )	average pore size (nm)	weight percentage from $\text{CO}_2$ adsorption	
				40 mL/min $\text{N}_2$ and 60 mL/min $\text{CO}_2$	40 mL/min air and 60 mL/min $\text{CO}_2$
sample A	irregular aggregates	3.44	8.84	113%	129%
sample B	irregular aggregates	2.77	18.88	114%	124%
sample C	nanowires	10.19	11.51	128%	130%
commercial (Fisher Scientific)	spherical aggregates	6.38	18.20	110%	118%

Figure 3. SEM images for  $\text{Li}_4\text{SiO}_4$  samples created using plasma oxidation: (a) sample A; (b) sample B; (c and d) sample C.

ratio 4:1 of Li–Si, and 1200 W plasma power; sample B was synthesized using Si nanopowder, a Li–Si molar ratio of 4:1, and 750 W plasma power, and finally sample C was made using Si nanopowder, an excess of lithium hydroxide (Li–Si of 8:1), and a plasma power of 750 W with indirect plasma flame exposure. See SI for more details on synthesis of lithium silicate aggregates and nanowire morphologies. From the XRD patterns, the percentage of  $\text{Li}_4\text{SiO}_4$  present was estimated through quantitative phase analysis based on reference intensity ratios with EVA software (Bruker). The capacity values are reported per gram of  $\text{Li}_4\text{SiO}_4$  phase present in the samples. For sample C a purity of 66.4% was found along with unreacted Si.

In the case of samples where lithium species other than silicates are present, it has been reported that the formation of an adsorption–desorption equilibrium between  $\text{Li}_2\text{CO}_3$  and  $\text{Li}_2\text{O}$  limits the weight loss above the desorption temperature.<sup>19</sup> Such behavior limits the cyclability of the materials containing unreacted or excess LiOH or  $\text{Li}_2\text{O}$  preventing their practical application. Samples synthesized with plasma oxidation where excess lithium species are not present were studied further in the present work.

Surface areas of various samples obtained were determined using BET (Brunauer–Emmett–Teller) measurements as described in the SI and presented in Figure S3. The  $\text{N}_2$  adsorption–desorption plot obtained using BET measurements

(Figure S3) displayed a type IV isotherm, with H3 type hysteresis. The absence of limiting adsorption at high  $P/P_0$  indicates the presence of slit-shaped pores, and the presence of hysteresis suggests capillary condensation related processes.<sup>20</sup> The results of the BET measurements are summarized in Table 1.

Scanning electron microscopy (SEM) analysis was performed as described in the SI. SEM images of sample A (Figure 3a) showed  $\text{Li}_4\text{SiO}_4$  agglomerates between 10 and 200  $\mu\text{m}$  as a general trend. SEM analysis of sample B (Figure 3b) showed 2–20  $\mu\text{m}$  particles, with an irregular shape distribution ranging from ricelike to fused sheets. The observed sheet morphology is consistent with the resulting  $\text{N}_2$  physisorption isotherm with H3 type hysteresis, suggesting capillary condensation with no limiting adsorption stage. SEM analysis of sample C (Figure 3c and d) indicated that it is composed of nanowire aggregates, with diameters less than 50 nm and lengths around 5  $\mu\text{m}$ .

The dynamic  $\text{CO}_2$  adsorption plots obtained under nitrogen environment for samples A, B, and C are shown in Figure 4a. The analysis procedure is detailed in the SI along with data on dynamic adsorption obtained in air environment (Figure S4). The thermograms presented in Figure 4 were collected in an environment containing 60 vol %  $\text{CO}_2$  in nitrogen with a total gas flow rate of 100 mL/min at temperatures ranging from 350 to 750  $^\circ\text{C}$ . The observed stepwise behavior in the dynamic

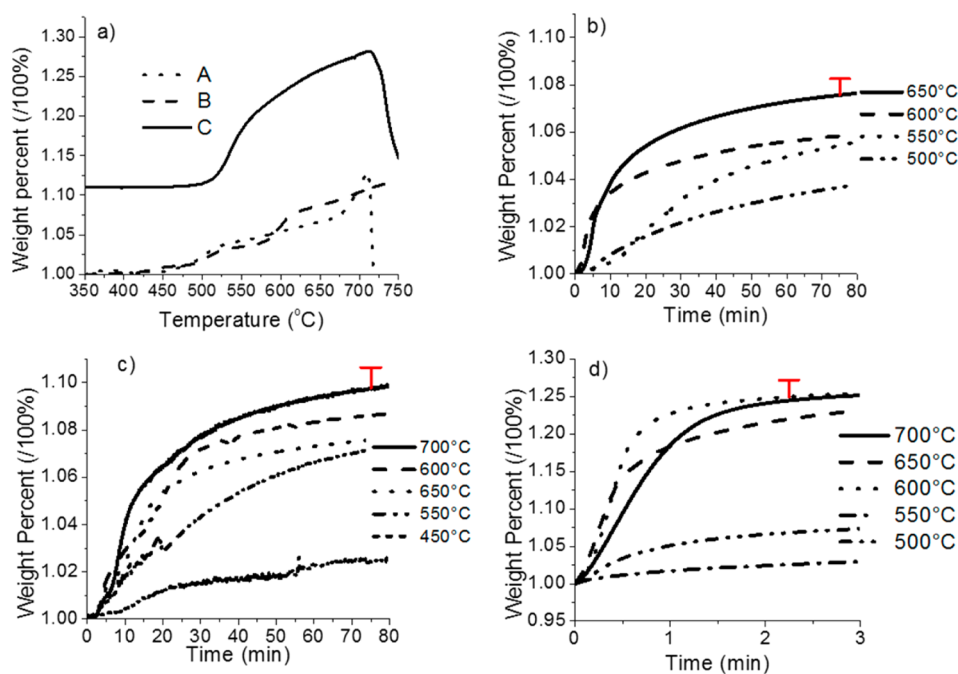


**Figure 4.** (a) CO<sub>2</sub> adsorption thermograms from samples A, B, and C under 60% CO<sub>2</sub> in nitrogen atmosphere at temperature ranges of 350–750 °C. Isotherms of CO<sub>2</sub> adsorption on Li-silicates (b) sample A, (c) sample B, and (d) sample C at different temperatures, under 60% CO<sub>2</sub> in nitrogen (100 mL/min).

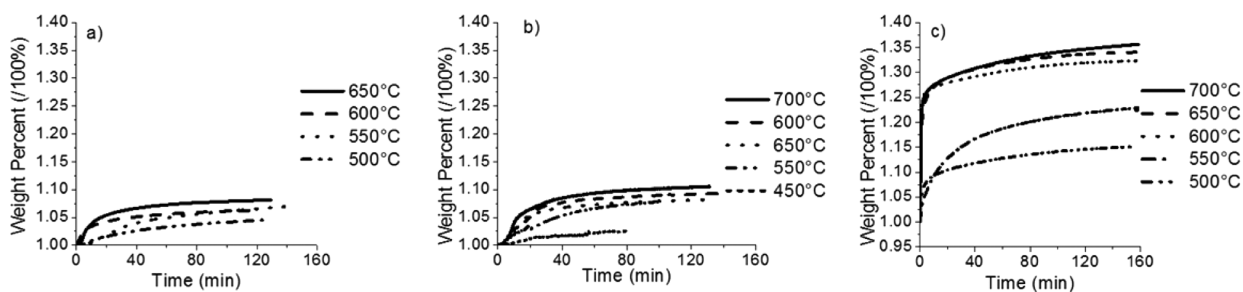


**Figure 5.** Full isotherms of CO<sub>2</sub> adsorption on Li silicates: (a) sample A, (b) sample B, and (c) sample C at different temperatures, under 60% CO<sub>2</sub> in nitrogen (100 mL/min).

adsorption data with samples A and B in Figure 4a is due to the experimental procedure used. In this experimental procedure, the mass flow rate was manually adjusted with a flow meter and a pressure gauge. Due to manual control, the highly sensitive microbalance showed stepwise behavior with weight increase due to adjustments of flow rates. For Sample C, the data were obtained using a mass flow controller resulting in smooth and continuous data. Even with the above limitation, the overall capacity values for samples A and B are not expected to be different than those reported here.

First and foremost, samples A and B exhibited stable thermograms at temperatures lower than 350 °C. In sharp contrast, sample C showed a partial adsorption process (Figures 4a and S4). From 350 to 500 °C, a slight weight increase (1–3%) can be observed in the samples. The main CO<sub>2</sub> adsorption process, however, seemed to occur at temperatures above 500 °C. All samples exhibited significant weight increments, reaching a maximum in the temperature range of 700–725 °C. Although the chemisorption process for all samples occurred from 500 °C under both N<sub>2</sub> and air environments, the maximum CO<sub>2</sub> adsorption temperatures were not the same under different carrier gases. For sample A,

under the pure N<sub>2</sub> environment, the CO<sub>2</sub> chemisorption occurred at the temperature range of 500–650 °C, and the maximum adsorption temperature was 700 °C. However, under air as the balance gas, the sample weight increased dramatically at 650–700 °C, and the CO<sub>2</sub> desorption began at 725 °C. For sample B, using N<sub>2</sub> as the carrier gas, the sample weight increase rate was stable from 500 to 750 °C, and it did not reach saturation under our experimental conditions. When studied under air atmosphere, sample B displayed an intense weight increase at 680–700 °C, and the CO<sub>2</sub> desorption process started at 725 °C. As for sample C, the performance of the material under different carrier gases was very similar. The initial stage of adsorption was below 350 °C, in the range of 100–300 °C; contrary to samples A and B that exhibited a highly active stage after 500 °C and slowly reached a maximum around 710 °C.

To estimate errors associated with the data shown in Figure 4, two sets of experiments were performed: First, the dynamic adsorption data curves were repeated several times for each sample and found the error based on CO<sub>2</sub> uptake to be less than 3%. Second, isotherms were obtained as a function of loading using 4.6 mg and 21.5 mg samples. The resulting data

showed no error in the initial time scales but started to show different saturation capacities; i.e., the smaller amount of sample exhibited higher saturation CO<sub>2</sub> uptake by about 6% compared to the sample with higher loading.

The CO<sub>2</sub> chemisorption does seem to depend not only on temperature, but also on the type of carrier gas. The O<sub>2</sub> from air seemed to benefit the carbonation process on the adsorbents at high temperatures. The CO<sub>2</sub> adsorption performance for the synthesized lithium silicate materials is compared against that of commercially available Li<sub>4</sub>SiO<sub>4</sub> (obtained from Fisher Scientific). The experimental results with CO<sub>2</sub> adsorption obtained using different lithium orthosilicate adsorbents are summarized in Table 1. The Li based adsorbents synthesized using the solvo-plasma technique exhibited better CO<sub>2</sub> sorption capacity than that of the commercial silicate in both N<sub>2</sub> and air environments.

The CO<sub>2</sub> sorption capacities of the synthesized materials are further studied by measuring isotherms at different temperatures. All of the isotherms exhibited exponential behavior with CO<sub>2</sub> adsorption, and higher CO<sub>2</sub> chemisorption capacities were observed when the samples were exposed to higher temperatures, as expected from the literature.<sup>21,22</sup>

As can be seen in Figure 5a–c where complete 160 min thermograms are shown, samples A and B reached the plateau behavior within 40 min at higher temperatures, while sample C reached this zone during the first minutes of the experiment with a sharp weight increase in the temperature range of 600–700 °C.

In contrast to the normal smooth transition depicting increasing CO<sub>2</sub> capacities with temperature, an “atypical capacity-switch” was observed in all samples around 600 °C, where a lower CO<sub>2</sub> capacity is obtained at a higher temperature, this “capacity switch” behavior has been reported earlier.<sup>23</sup> In short time scale, the rate of weight increase mainly depends on the CO<sub>2</sub> molecules being adsorbed on the Li<sub>4</sub>SiO<sub>4</sub> surface, whereas with a long time scale, it depends on the lithium diffusion to the particle surface.<sup>22</sup> Although a higher capacity and faster CO<sub>2</sub> chemisorption is expected for the Li silicate adsorbents, a range of temperatures from 550 to 650 °C is also associated with sintering of the Li silicate materials that can decrease the surface area and cycle life. Thus, the capacity switch is believed to be related to sintering phenomenon; i.e., when the sample temperature reaches the sintering point, the capacity decreases due to low surface CO<sub>2</sub> saturation, and the CO<sub>2</sub> sorption kinetics are enhanced beyond this temperature resulting in higher capacities. In our results, for sample A shown in Figure 4b the equilibrium isotherm curves at 600 and 550 °C described a convergent behavior, indicating that the capacity switch is further beyond 80 min, as can be seen in Figure 5a at around 90 min, the “capacity switch” took place between the two isotherms. The data for sample B show in Figure 4c that, although the adsorption rate (isothermal slope) was higher at 650 than 600 °C during the first 20 min, the final capacity at 650 °C was 0.076 g g<sup>-1</sup> lower than the 0.086 g g<sup>-1</sup> capacity obtained at 600 °C. The adsorption data obtained at 650 and 600 °C are shown in Figure 5b. The behavior of sample C was different in the first 3 min shown in Figure 4d; the CO<sub>2</sub> capacity switch is observed between 550 and 650 °C. The data show in Figure 5c that, over longer time scales, the CO<sub>2</sub> capacity increases with higher temperatures, indicating that nanowire powder sample (sample C) does not undergo sintering unlike spherical aggregates. The data with three samples containing different morphologies in terms of particle

size indicate that the capacity switch occurs at shorter times for smaller particles.

The nanostructured Li silicates synthesized using the solvo-plasma method exhibited higher CO<sub>2</sub> adsorption capacities than those obtained using conventional lithium silicate ceramics. For chemisorption, the CO<sub>2</sub> adsorption over the particle surface and the lithium diffusion are considered to be the rate-limiting steps of the whole CO<sub>2</sub> capture process. To study the whole adsorption processes, including the CO<sub>2</sub> adsorption and the lithium diffusion, all isotherms were fitted to a double-exponential model. The double-exponential equation is presented as

$$y = A \exp(-k_1x) + B \exp(-k_2x) + C \quad (1)$$

where  $y$  represents the weight percentage of CO<sub>2</sub> chemisorbed,  $x$  is the time, and  $k_1$  and  $k_2$  are the exponential parameters for the CO<sub>2</sub> adsorption, kinetically controlled by chemisorption and lithium diffusion processes respectively, over the surface of Li<sub>4</sub>SiO<sub>4</sub> particles or nanowires.  $A$  and  $B$  are constants, and  $C$  indicates the  $y$  axial intercept. Table 2 shows the kinetic parameters obtained from Li silicates isotherms fitted to the double-exponential model.

**Table 2. Kinetic Parameters Obtained from Li Silicate Adsorbents Isotherms at Different Adsorption Temperatures**

$T$ (°C)	$k_1$ (s <sup>-1</sup> )	$k_2$ (s <sup>-1</sup> )	$R^2$
Sample A			
500 °C	$1.71 \times 10^{-3}$	$3.94 \times 10^{-4}$	0.998
550 °C	$4.15 \times 10^{-3}$	$3.95 \times 10^{-4}$	0.99
600 °C	$4.53 \times 10^{-3}$	$4.79 \times 10^{-4}$	0.997
650 °C	$2.18 \times 10^{-3}$	$4.26 \times 10^{-4}$	0.996
Sample B			
550 °C	$5.32 \times 10^{-4}$	$5.04 \times 10^{-4}$	0.997
600 °C	$2.27 \times 10^{-3}$	$5.57 \times 10^{-4}$	0.989
650 °C	$1.13 \times 10^{-3}$	$5.11 \times 10^{-4}$	0.993
700 °C	$1.75 \times 10^{-3}$	$4.02 \times 10^{-4}$	0.994
Sample C			
500 °C	$3.05 \times 10^{-3}$	$3.89 \times 10^{-4}$	0.997
550 °C	$1.23 \times 10^{-2}$	$4.75 \times 10^{-4}$	0.999
600 °C	$3.55 \times 10^{-2}$	$3.43 \times 10^{-4}$	0.992
650 °C	$2.02 \times 10^{-2}$	$6.73 \times 10^{-4}$	0.989
700 °C	$2.16 \times 10^{-2}$	$3.60 \times 10^{-4}$	0.997

To explain the capacity and kinetic data, it is important to understand the basic mechanism involved with CO<sub>2</sub> sorption on Li<sub>4</sub>SiO<sub>4</sub> materials. As shown in Figure 6, the first step involves the reaction of CO<sub>2</sub> with Li atoms on the surface of the sorbent creating a coating of Li<sub>2</sub>CO<sub>3</sub> under a pure chemisorption controlled step. Once this layer is completely formed, new Li atoms need to diffuse throughout the carbonate layer to reach the surface and react with the CO<sub>2</sub> in a diffusion controlled stage.<sup>24</sup> The samples A and B exhibited similar  $k_1$  values, while sample C exhibited an order of magnitude higher  $k_1$  values. The isotherm data in Figure 4d clearly indicate that the CO<sub>2</sub> dramatically increased for nanowire sample within a minute confirming that the entire sorption process is controlled by surface reaction process as shown in Figure 6. The  $k_2$  values are on the same order of magnitude for all samples implying similar mechanisms for the diffusion of Li through Li<sub>2</sub>CO<sub>3</sub> formed on the surface of the particle or nanowire as shown in Figure 6. These results are in good agreement with the data

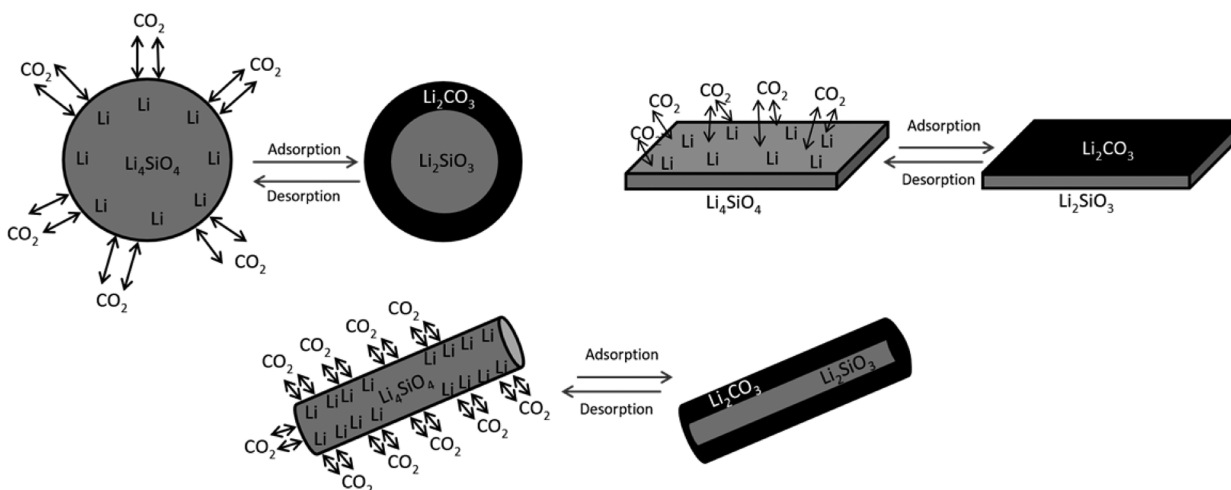


**Figure 6.** Schematics illustrating a comparison of CO<sub>2</sub> adsorption mechanisms within lithium silicate materials with different morphologies.

from the literature,<sup>14,25</sup> for samples A and B. Sample C exhibited an order of magnitude higher  $k_1$  values suggesting highly active surface over the entire temperature range. Moreover, the dynamic adsorption results in Figure 4a show the adsorption for the lithium orthosilicate nanowires started at much lower temperatures than the typical adsorption starting temperature of 500 °C.

Using the CO<sub>2</sub> adsorption isotherms, the activation energy in Sample C can be estimated to be close to 66 kJ/mol, slightly lower than values reported in the literature (70–105 kJ/mol).<sup>14,26</sup> It is believed that the change in chemisorption activation energy with the morphology is due to a change in reactivity caused by a higher number of lithium atoms on the surface of the material.<sup>24</sup> The mechanistic detail shown in Figure 6 can be extended to Li<sub>2</sub>SiO<sub>3</sub> nanowires. The CO<sub>2</sub> sorption on to Li<sub>2</sub>SiO<sub>3</sub> nanowire will lead to silica core and Li<sub>2</sub>CO<sub>3</sub> shell formation which can make it difficult to be reversed upon desorption of CO<sub>2</sub>.

The cyclability of CO<sub>2</sub> sorption and desorption for nanowires sample is shown in Figure 7. The most drastic

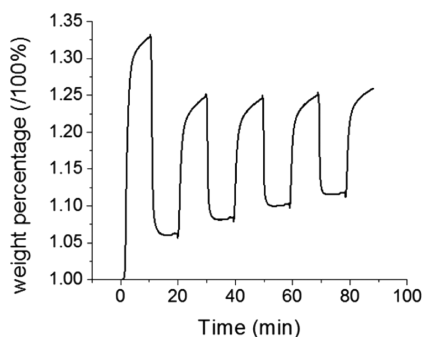


**Figure 7.** Cyclability of lithium orthosilicate nanowires under 40 mL/min N<sub>2</sub> and 60 mL/min CO<sub>2</sub>, adsorption temperature of 700 °C, and desorption temperature of 720 °C.

decrease with capacity happens during the second adsorption step, where the uptake goes from 33% for first cycle down to 25% for the second one and stays approximately constant for the rest of the cycles of adsorption–desorption. Incomplete desorption due to the limitations of the experimental setup used are believed to be responsible for the observed decrease. In addition, the use of a low desorption temperature may have

contributed to incomplete desorption. As the nanowire powder sample was held in a pan, the sample holder shape with inaccessible regions for CO<sub>2</sub>/carrier gas flow and the packing of the sample could have contributed to the observed decrease in subsequent cycles. Nevertheless, the data show significant reversibility with fast CO<sub>2</sub> sorption and desorption kinetics. Dynamic adsorption–desorption experiments using a fixed-bed or fluidized bed could mitigate the above factors.

In summary, in the present work different morphologies for lithium silicates (nanoparticles, sheets, and nanowires) were synthesized using a new type of process using plasma oxidation with reaction time scales of about a minute. These materials were used in CO<sub>2</sub> sorption experiments to understand their capacity and kinetics, results suggested that all samples synthesized in this study could lead to a higher CO<sub>2</sub> uptake than commercially available lithium silicate (18% uptake). Subsequent analysis indicated that the lithium diffusion occurred in the same fashion according to  $k_2$  while the distances of this process varied greatly throughout samples, reaching 25 nm in the nanowire sample (radius) providing a fast lithium supply to the surface for this morphology. The sorption capacity of 25% by wt within a time scale of just 3 min demonstrates that nanowire morphology leads to an ultrafast CO<sub>2</sub> adsorption, radically decreasing 2 orders of magnitude the time scales when compared to all other morphologies and also exhibited sorption capacity close to theoretical values. Moreover, the synthesis of nanowire morphologies through our plasma oxidation technique leads to a fast scalable way to obtain material targeting systems where diffusion barriers are detrimental.

## ■ ASSOCIATED CONTENT

### 📄 Supporting Information

The Supporting Information is available free of charge on the ACS Publications website at DOI: 10.1021/acs.nanolett.6b04013.

Methodology followed for the synthesis of lithium silicates with the solvo-plasma technique, characterization of synthesized materials, CO<sub>2</sub> adsorption studies, CO<sub>2</sub> thermograms (PDF)

## ■ AUTHOR INFORMATION

## Corresponding Author

\*E-mail: mahendra@louisville.edu.

ORCID 

Mahendra Sunkara: 0000-0003-2087-5261

## Notes

The authors declare no competing financial interest.

## ■ ACKNOWLEDGMENTS

We acknowledge partial support from NSF EPSCoR (1355438), Conn Center for Renewable Energy Research, and Department of Chemical Engineering at University of Louisville.

## ■ REFERENCES

- (1) Wei, C.-C.; Puxty, G.; Feron, P. Amino acid salts for CO<sub>2</sub> capture at flue gas temperatures. *Chem. Eng. Sci.* **2014**, *107*, 218–226.
- (2) Xiang, S.; He, Y.; Zhang, Z.; Wu, H.; Zhou, W.; Krishna, R.; Chen, B. Microporous metal-organic framework with potential for carbon dioxide capture at ambient conditions. *Nat. Commun.* **2012**, *3*, 954.
- (3) Shan, S.; Jia, Q.; Jiang, L.; Li, Q.; Wang, Y.; Peng, J. Novel Li<sub>4</sub>SiO<sub>4</sub>-based sorbents from diatomite for high temperature CO<sub>2</sub> capture. *Ceram. Int.* **2013**, *39* (5), 5437–5441.
- (4) Leung, D. Y.; Caramanna, G.; Maroto-Valer, M. M. An overview of current status of carbon dioxide capture and storage technologies. *Renewable Sustainable Energy Rev.* **2014**, *39*, 426–443.
- (5) McDonald, T. M.; Mason, J. A.; Kong, X.; Bloch, E. D.; Gygi, D.; Dani, A.; Crocella, V.; Giordanino, F.; Odoh, S. O.; Drisdell, W. S.; Vlaisavljevich, B.; Dzubak, A. L.; Poloni, R.; Schnell, S. K.; Planas, N.; Lee, K.; Pascal, T.; Wan, L. F.; Prendergast, D.; Neaton, J. B.; Smit, B.; Kortricht, J. B.; Gagliardi, L.; Bordiga, S.; Reimer, J. A.; Long, J. R. Cooperative insertion of CO<sub>2</sub> in diamine-appended metal-organic frameworks. *Nature* **2015**, *519* (7543), 303–308.
- (6) Ávalos-Rendón, T.; Casa-Madrid, J.; Pfeiffer, H. Thermochemical capture of carbon dioxide on lithium aluminates (LiAlO<sub>2</sub> and Li<sub>5</sub>AlO<sub>4</sub>): a new option for the CO<sub>2</sub> absorption. *J. Phys. Chem. A* **2009**, *113* (25), 6919–6923.
- (7) Jana, S.; Das, S.; Ghosh, C.; Maity, A.; Pradhan, M. Halloysite Nanotubes Capturing Isotope Selective Atmospheric CO<sub>2</sub>. *Sci. Rep.* **2015**, *5*, 8711.
- (8) Ochoa-Fernández, E.; Rønning, M.; Grande, T.; Chen, D. Synthesis and CO<sub>2</sub> capture properties of nanocrystalline lithium zirconate. *Chem. Mater.* **2006**, *18* (25), 6037–6046.
- (9) Rodríguez-Mosqueda, R.; Pfeiffer, H. Thermokinetic analysis of the CO<sub>2</sub> chemisorption on Li<sub>4</sub>SiO<sub>4</sub> by using different gas flow rates and particle sizes. *J. Phys. Chem. A* **2010**, *114* (13), 4535–4541.
- (10) Yi, K. B.; Eriksen, D. Ø. Low temperature liquid state synthesis of lithium zirconate and its characteristics as a CO<sub>2</sub> sorbent. *Sep. Sci. Technol.* **2006**, *41* (2), 283–296.
- (11) Kato, M.; Nakagawa, K.; Essaki, K.; Maezawa, Y.; Takeda, S.; Kogo, R.; Hagiwara, Y. Novel CO<sub>2</sub> Absorbents Using Lithium-Containing Oxide. *Int. J. Appl. Ceram. Technol.* **2005**, *2* (6), 467–475.
- (12) Duan, Y.; Pfeiffer, H.; Li, B.; Romero-Ibarra, I. C.; Sorescu, D. C.; Luebke, D. R.; Halley, J. W. CO<sub>2</sub> capture properties of lithium silicates with different ratios of Li<sub>2</sub>O/SiO<sub>2</sub>: an ab initio thermodynamic and experimental approach. *Phys. Chem. Chem. Phys.* **2013**, *15* (32), 13538–13558.
- (13) Carella, E.; Hernandez, M. High lithium content silicates: A comparative study between four routes of synthesis. *Ceram. Int.* **2014**, *40* (7), 9499–9508.
- (14) Subha, P. V.; Nair, B. N.; Hareesh, P.; Mohamed, A. P.; Yamaguchi, T.; Warriar, K. G. K.; Hareesh, U. S. Enhanced CO<sub>2</sub> absorption kinetics in lithium silicate platelets synthesized by a sol-gel approach. *J. Mater. Chem. A* **2014**, *2* (32), 12792–12798.
- (15) Pfeiffer, H.; Bosch, P.; Bulbulian, S. Synthesis of lithium silicates. *J. Nucl. Mater.* **1998**, *257* (3), 309–317.
- (16) Tang, T.; Zhang, Z.; Meng, J.-B.; Luo, D.-L. Synthesis and characterization of lithium silicate powders. *Fusion Eng. Des.* **2009**, *84* (12), 2124–2130.
- (17) Kumar, V.; Kim, J. H.; Jasinski, J. B.; Clark, E. L.; Sunkara, M. K. Alkali-assisted, atmospheric plasma production of titania nanowire powders and arrays. *Cryst. Growth Des.* **2011**, *11* (7), 2913–2919.
- (18) Nguyen, T. Q.; Atla, V.; Vendra, V. K.; Thapa, A. K.; Jasinski, J. B.; Druffel, T. L.; Sunkara, M. K. Scalable solvo-plasma production of porous tin oxide nanowires. *Chem. Eng. Sci.* **2016**, *154*, 20–26.
- (19) Mosqueda, H. A.; Vazquez, C.; Bosch, P.; Pfeiffer, H. Chemical Sorption of Carbon Dioxide (CO<sub>2</sub>) on Lithium Oxide (Li<sub>2</sub>O). *Chem. Mater.* **2006**, *18* (9), 2307–2310.
- (20) Thommes, M.; Kaneko, K.; Neimark, A. V.; Olivier, J. P.; Rodríguez-Reinoso, F.; Rouquerol, J.; Sing, K. S. W. Physisorption of gases, with special reference to the evaluation of surface area and pore size distribution (IUPAC Technical Report). *Pure Appl. Chem.* **2015**, *87*, 1051.
- (21) Ortiz-Landeros, J.; Romero-Ibarra, I. C.; Gómez-Yáñez, C.; Lima, E.; Pfeiffer, H. Li<sub>4+x</sub>(Si<sub>1-x</sub>Al<sub>x</sub>)O<sub>4</sub> Solid Solution Mechanosynthesis and Kinetic Analysis of the CO<sub>2</sub> Chemisorption Process. *J. Phys. Chem. C* **2013**, *117* (12), 6303–6311.
- (22) López Ortiz, A.; Escobedo Bretado, M. A.; Guzmán Velderrain, V.; Meléndez Zaragoza, M.; Salinas Gutiérrez, J.; Lardizábal Gutiérrez, D.; Collins-Martínez, V. Experimental and modeling kinetic study of the CO<sub>2</sub> absorption by Li<sub>4</sub>SiO<sub>4</sub>. *Int. J. Hydrogen Energy* **2014**, *39* (29), 16656–16666.
- (23) Quinn, R.; Kitzhoffer, R. J.; Hufton, J. R.; Golden, T. C. A High Temperature Lithium Orthosilicate-Based Solid Absorbent for Post Combustion CO<sub>2</sub> Capture. *Ind. Eng. Chem. Res.* **2012**, *51* (27), 9320–9327.
- (24) Venegas, M. J.; Fregoso-Israel, E.; Escamilla, R.; Pfeiffer, H. Kinetic and reaction mechanism of CO<sub>2</sub> sorption on Li<sub>4</sub>SiO<sub>4</sub>: study of the particle size effect. *Ind. Eng. Chem. Res.* **2007**, *46* (8), 2407–2412.
- (25) Wang, K.; Zhao, P.; Guo, X.; Li, Y.; Han, D.; Chao, Y. Enhancement of reactivity in Li<sub>4</sub>SiO<sub>4</sub>-based sorbents from the nano-sized rice husk ash for high-temperature CO<sub>2</sub> capture. *Energy Convers. Manage.* **2014**, *81* (0), 447–454.
- (26) Shan, S.; Jia, Q.; Jiang, L.; Li, Q.; Wang, Y.; Peng, J. Preparation and kinetic analysis of Li<sub>4</sub>SiO<sub>4</sub> sorbents with different silicon sources for high temperature CO<sub>2</sub> capture. *Chin. Sci. Bull.* **2012**, *57* (19), 2475–2479.